coatings

MDPI

Article

A Single-Ended Ultra-Thin Spherical Microbubble Based on the Improved Critical-State Pressure-Assisted Arc Discharge Method

Wenfeng Guo [1,2,†], Jianxun Liu [3,4,†], Jinrong Liu [5], Gao Wang [2], Guanjun Wang [3,*] and Mengxing Huang [3,*]

1 School of Equipment Engineering, Shenyang Ligong University, Shenyang 110159, China; shirly-guo@139.com
2 College of Information and Communication Engineering, North University of China, Taiyuan 030051, China; wanggao@nuc.edu.cn
3 Collage of Information Science & Technology, Hainan University, Haikou 570228, China; 993802@hainu.edu.cn
4 Hainan Science & Technology Department, Haikou 570228, China
5 School of Optoelectronic Science and Engineering, University of Electronic Science and Technology of China, Chengdu 611731, China; liujinrong337@gmail.com
* Correspondence: wangguanjun@hainu.edu.cn (G.W.); huangmx09@hainu.edu.cn (M.H.)
† These authors contributed equally to this work.

Received: 29 January 2019; Accepted: 19 February 2019; Published: 22 February 2019

Abstract: Hollow core microbubble structures are good candidates for the construction of high performance whispering gallery microresonator and Fabry-Perot (FP) interference devices. In the previous reports, most of interest was just focused on the dual-ended microbubble, but not single-ended microbubble, which could be used for tip sensing or other special areas. The thickness, symmetry and uniformity of the single-ended microbubble in previous reports were far from idealization. Thus, a new ultra-thin single-ended spherical microbubble based on the improved critical-state pressure-assisted arc discharge method was proposed and fabricated firstly in this paper, which was fabricated simply by using a commercial fusion splicer. The improvement to former paper was using weak discharge and releasing pressure gradually during the discharging process. Thus, the negative influence of gravity towards bubble deformation was decreased, and the fabricated microbubble structure had a thin, smooth and uniform surface. By changing the arc discharge parameters and the fiber position, the wall thicknesses of the fabricated microbubble could reach the level of 2 μm or less. The fiber Fabry-Perot (FP) interference technique was also used to analyze the deformation characteristic of microbubble under difference filling pressures. Finding the ends of the microbubbles had a trend of elongation with axial compression when the filling pressure was increasing. Its sensitivity to the inner pressure of microbubble samples was about ~556 nm/MPa, the bubble wall thickness was only of about 2 μm. Besides, a high whispering gallery mode (WGM) quality factor that up to 10^7 was realized by using this microbubble-based resonator. To explain the upper phenomenon, the microbubble was modeled and simulated with the ANSYS software. Results of this study could be useful for developing new single-ended whispering gallery mode micro-cavity structure, pressure sensors, etc.

Keywords: fiber optics sensor; Fabry-Perot; whispering gallery mode; microresonator

1. Introduction

Microbubble could be very useful in many optical fiber sensing applications [1]. For example, a high sensitivity pressure sensor based on the Fabry-Perot (FP) interference could be realized by

using hollow microbubble structure [2]. Such structure could be used for the blood oxygen degree measurement. Meanwhile, the thin ring structure that makes the bubble could be applied for highly sensitive pressure measurement [3].

Microbubble could be divided into two kinds: The dual-ended microbubble and the single-ended microbubble. Recently, dual-ended microbubble with ultra-high quality value is considered as excellent opto-microfluidic devices [4–8] and high performance optical sensors, such as strain [9], bio/chemical [10] and temperature [11] sensing, and lasing [12]. Correspondingly, the pressure-assisted discharging and pressure-assisted CO_2 micro-machining methods were proposed for fabricating such dual-ended microbubble. The fabrication of ultrathin-walled (approaching 500 nm), silica dual-ended microbubbles with Q-factors of about 10^7 at the telecommunications C-band has been reported [13].

On the contrary, the fabrication method of single-ended microbubble was far from ideal [14–18]. In 2011, Amy Watkins presented a single-input whispering gallery optical microbubble resonator by heating the tapered tip of a pressurized glass capillary using a CO_2 laser. However, due to its imperfect symmetry, the optical whispering gallery modes with Q factors were only of 10^5 [14]. Rico Henze demonstrated another single-ended microbubble for whispering gallery mode (WGM). By changing the inner aerostatic pressure, an absolute resonance shifts of hundreds of GHz corresponding to tuning pressure ranges has been observed. But the extra-thick end face makes it unsuitable for tip FP sensing [15]. It should be noted that the upper two papers were published in 2011. Their shortcoming is that the bubble surface, especially the end surface, is thicker, uneven, not smooth, and asymmetric. To the best of our knowledge, no other reports that are similar to upper single-ended microbubble have been published from 2012 to 2017. We think the reason is that there is no mature method for fabricating such single-ended hollow core microbubble.

It is believed that, for the solid core microsphere microresonators, the melting shrinkage effect will occur when the electronic arc is discharged, which will contribute to form the solid core microsphere microresonator with good smoothness and uniformity [19]. While for hollow core microbubble microresonator, when the filling pressure is relatively too high, the radius of microbubble will expand (that is, the expansion state), but when the filling pressure is relatively too low, the shrinkage effect could occur (that is, the contraction state). Supposing the discharge and filling pressure is controlled at a reasonable state, a transitional critical state between expansion state and contraction state exists. Under the condition of critical-state pressure-assisted arc discharge by repeatedly regulating and controlling the parameters of discharge intensity, filled air pressure value, microbubble position and others, the microbubble film layer can be gradually thinned, and at the same time, the advantages of the traditional solid microsphere cavity are smooth, uniform and symmetry could be retained.

Finally, this improved critical-state pressure-assisted arc discharge method was proposed for fabricating ultra-thin single-ended hollow core microbubble structure here. This method possesses the merits of using weak discharge and releasing pressure gradually during the discharge process. Thus, the negative influence of gravity on bubble deformation during the arc discharge process was avoided at the best. Finally, the fabricated microbubble has a thin, smooth and uniform surface. The final wall thickness of the microbubbles would be as low as ~2 μm or less. In addition, its mechanical property was also analyzed by utilizing the FP interference method. The strain sensitivity to the inner pressure of microbubbles samples of about ~556 nm/MPa was proved in this experiment. As well, a high WGM quality factor up to 10^7 was also calculated. To explain the upper experiment results, the mechanical properties of the fabricated microbubble were also simulated with ANSYS software. Finally, the focus of this paper is to optimize the fabrication of single-ended bubbles using only the improved critical-state pressure-assisted arc discharge method at a very cheap cost.

2. Fabrication Process and Results

In the previous study, it is found that for solid microsphere materials, the melt-shrinkage effect occurs during arc discharge, which results in a solid microsphere cavity with good smoothness and uniformity. For hollow microbubble materials, when the filling gas pressure is relatively large,

the microbubbles will expand (i.e., expand state); when the filling gas pressure is too small, shrinkage (i.e., shrinkage state) will occur.

Further in-depth analysis found that the filling gas pressure and melting discharge parameters are the key to the preparation of ultra-thin microbubbles. The general view is that when the filling pressure is large, the microbubbles will be thinned more quickly. However, considering the existence of factors such as gravity and uneven discharge, excessive filling pressure can cause distortion or even rupture of the microbubbles. If the filling pressure is too small, the expansion effect of the microbubbles will be minimal.

In the experimental study on the preparation of microbubbles by expansion-assisted discharge, there is a transitional critical state between the expanded state and the contracted state under the conditions of reasonable regulation of discharge and filling pressure to the best of our knowledge. In the case of a critical state pressure-asssisted arc discharge, appropriately increasing the filling gas pressure causes the microbubbles to slowly expand, eventually making the film layer thin. Moderately reducing the filling gas pressure is going to cause the microbubbles to shrink slowly, and the uniformity and symmetry of the film layer will be improved. By repeatedly adjusting the parameters such as discharge, filling pressure, and microbubble position, not only the microbubble layer is gradually thinned, but also the advantages of smooth and uniform symmetry of the conventional solid microsphere cavity can be retained. This method can provide a unique solution for the improvement of microbubble microcavity dispersion and quality factor characteristics.

The proposed hollow core single-ended microbubble was fabricated by using the improved critical-state pressure-assisted arc discharge method. The main fabrication process was depicted in Figure 1. The silica hollow core tube used here has 125 μm outer diameter, 75 μm inner diameter. The plastic coating of the tube was removed before fusion. An optical fiber fusion splicer (60s, Fujikura, Tokyo, Japan) was adopted to generate the arc discharge. A pressure pump (Kangsite Instrument ConST162, ConST, Beijing, China) was used to produce high pressure air to the hollow core of the silica tube.

As it is depicted in Figure 1, first, one end of the hollow core tube was connected to the pressure pump. The other end was fused with a single mode fiber. Second, an about 120 kPa atmospheric pressure was delivered from the pressure pump to the tube. Meanwhile, the other end of tube was melted with a discharging time of 300 ms and a discharging intensity of −5 bits. A pulling force was also enforced by tuning the motors of fusion splicer. Then, two triangular tips were formed. Third, the hollow core tip was removed to the left side of the electrode, and re-discharged 3–5 times again under the condition of filling the tube with high pressure air. A microbubble with relatively thick wall would be generated at the end of silica tube. Finally, the position of microbubble was slightly moved to the heating region, and discharged again under the condition of filling the tube with high pressure air. After a few times of discharge, the microbubble would experience more expansion, and its wall thickness would reach to several micrometers, and possess a uniform feature at the same time.

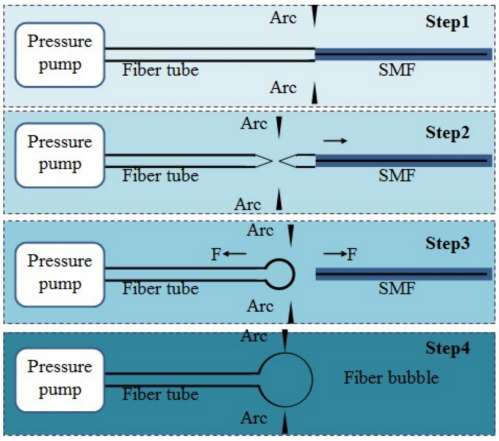

Figure 1. Fabrication processes of the proposed single-ended microbubble.

Figure 2 depicted the results of the fabrication process in each step. Figure 2a was the shape of silica tube and single mode fiber after the first fusion, and Figure 2b was the microscopy photograph of the produced triangular tip. Figure 2c is the preliminary structure of fabricated microbubble after the third step, which shows that the wall of the microbubble was thick. Figure 2d shows the 20× microscopic image of the fabricated single-ended microbubble. The experiment proved that using the upper improved fabrication method, the negative influence of gravity on bubble deformation during the arc discharge process was avoided at the best. The wall thickness could reach the value of ~2 μm or less, which was measured under the following SEM experiment.

It needs to be emphasized that the uniformity of the original microbubble was especially important to fabricating the final ultrathin single-ended microbubble. Unsuitable original structure would enhance the negative influence of gravity and bring the experiment to failure, as is shown in Figure 3a. Figure 3b is the image of a broken microbubble, which is formed due to the non-uniform wall thickness. We can imagine that such kind of microbubble would be broken after several times of arc discharge under the high filling pressure air.

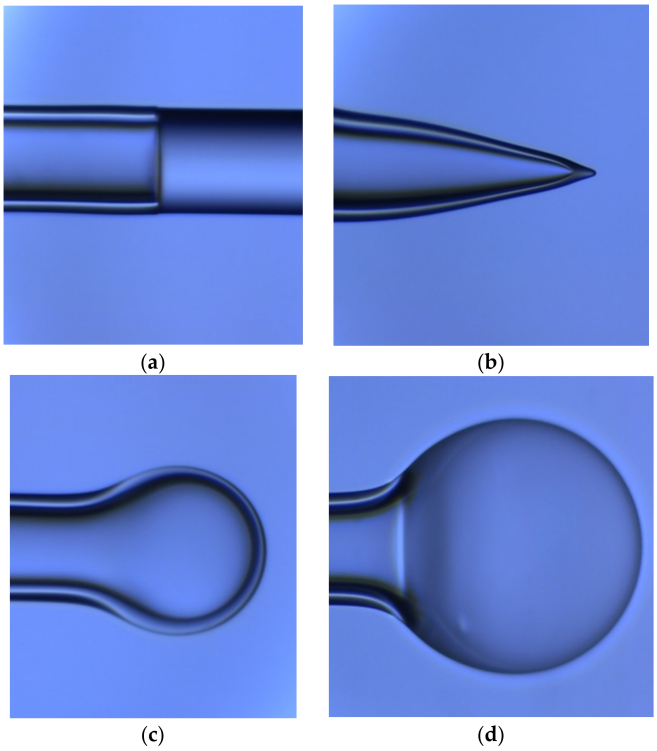

Figure 2. Fabrication results in each step. (**a**) First step; (**b**) second step; (**c**) third step; (**d**) fourth step.

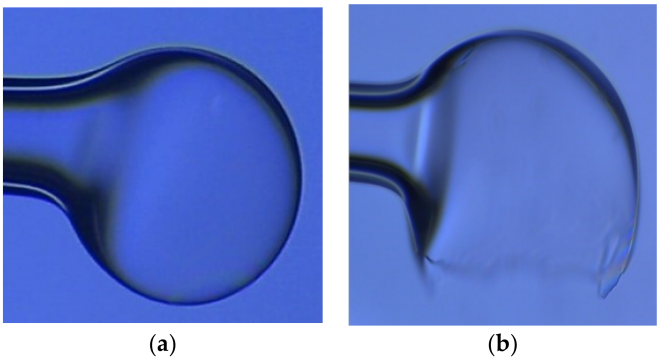

Figure 3. Failed experiment and the specific reason. (**a**) Deformation due to the gravity; (**b**) deformation due to non-uniform wall thickness.

For measuring the wall thickness of the fabricated microbubble, a SEM test (s-4800, HITACHI, Tokyo, Japan) was carried out after the fabrication process. The microbubble was broken with a mechanical method firstly, and then vertically placed into the electron microscope cavity. Experiment results were shown in Figure 4. It can be concluded that: 1. The structure of the microbubble was symmetrical, with less distortion; 2. the wall thickness of the microbubble was relatively uniform. 3. as was shown in Figure 4b, the wall thickness of the micro bubble was about 2 μm. While compared with the previous experiment result of Henze and Watkins [14,15], the microbubble here has the advantages in terms of symmetry, uniformity and wall thickness. It is believed that the improvement of this paper is the optimization of the single-end bubble manufacturing method, that is, to gradually weaken the discharge and release the pressure during the discharge process. Thus, the negative influence of gravity on bubble deformation during the arc discharge process is avoided at the best. As a result, the fabricated bubble structure has a thin, smooth and uniform surface. Furthermore, the fabrication cost is very cheap, since only a commercial fusion splicer is used here to fabricate such microbubble.

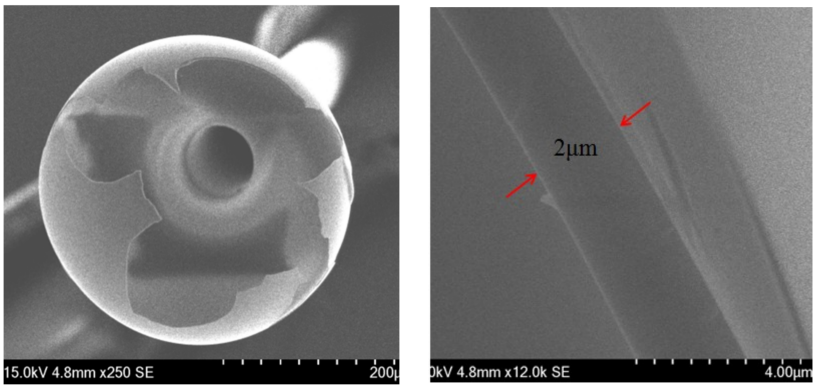

(**a**) (**b**)

Figure 4. Result of SEM experiment. (**a**) Collapsed single-ended microbubble; (**b**) measured wall thickness.

3. Mechanical Properties and Analysis

This thin and uniform single-ended microbubble could be very useful for FP cavity-based pressure sensors and WGM based devices. For example, when the inner wall of microbubble was filled with air of different pressures, the position of the silica bubble tip will move due to the thin and elastic characteristic. As the deformation degree was related with the shift of interference spectrum and pressure sensitivity, decreasing the thickness and expanding area of the end film contributes to sensitivity enhancement. For detecting the specific relationship of bubble parameter and pressure sensitivity, an experimental setup as shown in Figure 5 was used to analyze the mechanical characteristics of the tip deformation of the single-ended microbubble based on the FP interference principle. The corresponding measurement system includes an ASE light source with intensity of I_0, a circulator, and an optical spectrum analyzer (si320, Micron Optics, Atlanta, GA, USA). One reflection beam with intensity of I_1 comes from the single mode fiber tip and the other reflection beam with intensity of I_2 comes from the end face of microbubble. The FP interference was constituted between the two beams. Microbubble sample in Figure 2d was used in the measurement experiments, while the pressure unit used here was the absolute pressure. The atmospheric pressure was filled into the microbubble from a pressure pump through the glass tube.

Figure 6 shows the FP interference spectrum of the single-ended microbubble under different filling air pressures (from 4 to 1400 kPa). Here the distance d between the singe-ended bubble and fiber-end was fixed at near 30 μm. By adjusting the pitch distance, the interference spectrum will change correspondingly. By analyzing the relationship of the spectrum peak wavelength shift and the different filling pressures, the mechanical deformation characteristics of fabricated single-ended microbubble could be calculated.

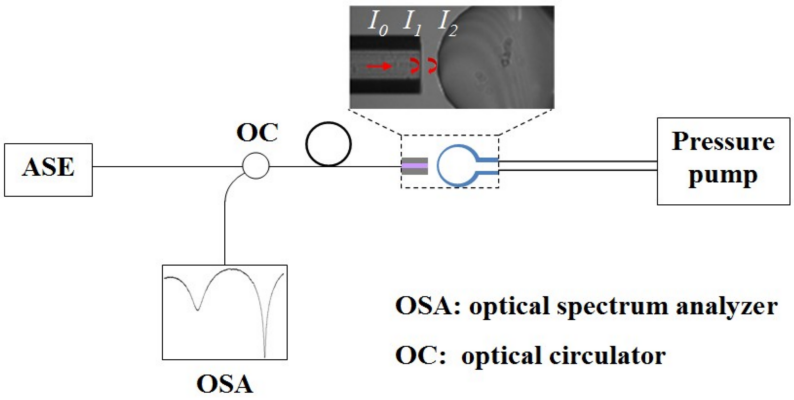

Figure 5. Experimental setup for measuring the pressure sensitity of the fabricated single-ended microbubble.

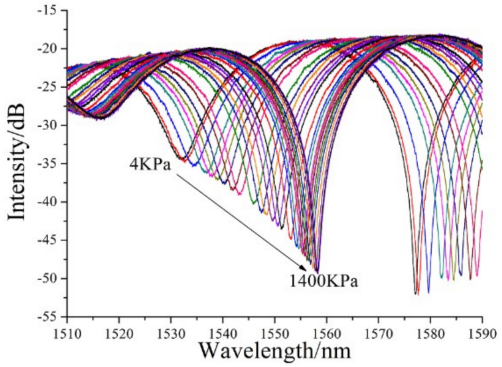

Figure 6. FP interference spectrum of the microbubbles.

Figure 7 depicts the relationship of peak wavelength shift and filling pressure. The measured pressure range was from 4 to 1400 kPa. It can be seen from Figure 7 that the peak wavelength of the interference spectra has experienced a red-shift with the increase of filling air pressure. But it seems that when the inner pressure was more than 800 kPa, the sensitivity to pressure will be decreased. In my opinion, the main reason may be that the thickness of fabricated was uniform relatively and it was easier to reach the nonlinear deformation region according the theory of elasticity, which has been explained in reference [20,21]. It can be assumed that when the filling pressure reaches a certain degree, relationship of filling pressure and bubble deformation will become too complex to attain a linear relationship. Besides, the maximum filling pressure is higher than 2000 kPa before the rupture of microbubble. As the filling pressure becomes unstable when it exceeds 1400 kPa by the utilized pressure pump, the influence of higher pressure than 1400 kPa on microbubble is not calculated here.

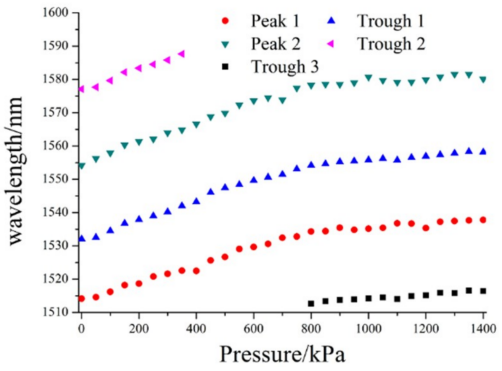

Figure 7. Relationship peak wavelength shift and filling pressure.

According to the relationship of pitch distance d and the FP interference peak λ_1, λ_2,

$$d = \lambda_1\lambda_2/2(\lambda_1 - \lambda_2) \quad (1)$$

the relationship of pitch distance d and the filling pressure could be calculated, which was depicted in Figure 8. It seems that, when the filling pressure range was from 4 to 800 kPa, the deformation sensitivity of the fabricated single-ended microbubble to filling pressure was about 556 nm/MPa in terms of cavity length change. Also, when the filling pressure ranges from 800 to 1400 kPa, the deformation sensitivity of the fabricated single-ended microbubble to filling pressure was about 98 nm/MPa in terms of cavity length change. As the peak wavelength was obtained by numerical fitting with a certain degree of deviation, the linearity of the pressure sensitivity data was not good, relatively.

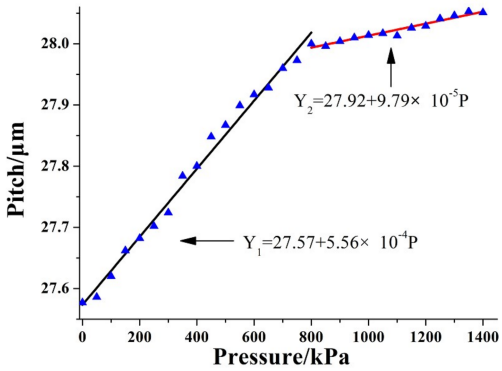

Figure 8. The relationship of pitch distance d and the filling pressure.

For analyzing the WGM quality factor characteristic of the proposed single-ended microbubble, a whispering gallery mode agitation and coupling experiment was also operated subsequently. Figure 9a depicts the experimental platform of whispering gallery mode agitation and coupling system. A tapered fiber with waist diameter of nearly 2 μm was used to stimulate the WGM mode, and the central wavelength and bandwidth of the DFB laser source were 1550 nm and 80 pm, respectively. Figure 9b was the screen shot of the corresponding output spectrum of WGM mode. A triangular wave voltage was used here to tune the laser wavelength, and a high-speed photodetector was used here to detect the intensity variety of the DFB laser. It could be seen from the Figure 4b that a sharp WGM resonant loss peak in the output spectrum appeared due to the interference effect of WGM mode.

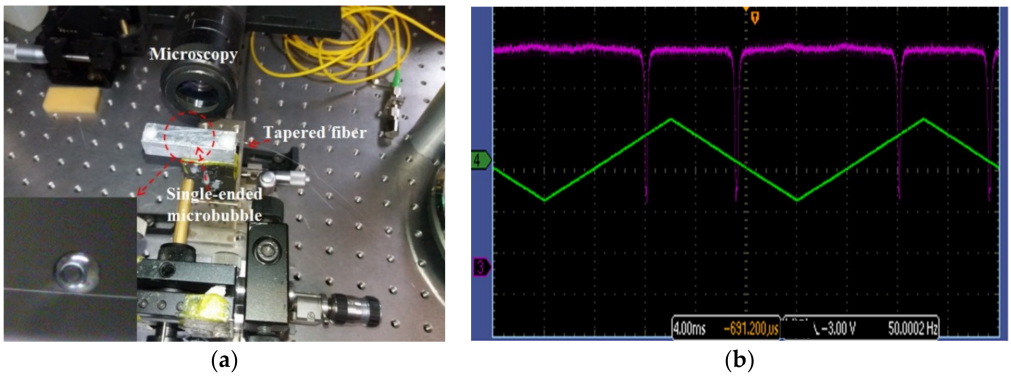

(**a**) (**b**)

Figure 9. Experimental system and the output WGM spectrum. (**a**) Experimental setup of the WGM system; (**b**) screen shot of the output spectrum.

The output spectrum of the fabricated single-ended microbubble WGM sensor was calculated and analyzed subsequently, which is shown in Figure 10. The corresponding full width at half maximum (FWHM) could be calculated as nearly 0.15 pm. According to the formula of quality factor

$Q = \Delta\lambda/\lambda$, the quality factor of fabricated fiber bubble WGM micro-resonator can reach to 10^7. Thus, this high quality factor characteristic has a significant advantage in many WGM micro-resonator sensing applications, such as pressure sensing, biochemical sensing and so on.

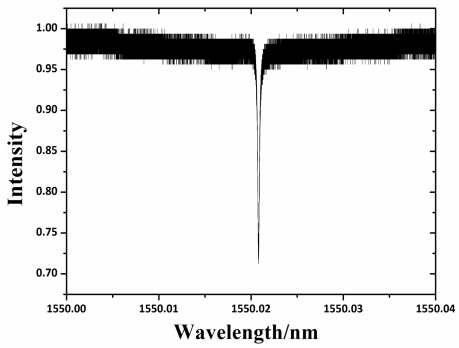

Figure 10. Output spectrum of the proposed single-ended microbubble-based WGM resonator.

For analyzing the relationship of bubble thickness and the filled pressure, the ANSYS software (v16.0) was used to model the microbubbles and simulate the deformation of microbubble under difference filling pressure. As was depicted in Figure 11, different parts of the single microbubble suffered different deformation under the same inner air pressure. When the filling absolute air pressure is close to zero, the end face of microbubble suffers to the inner direction, while the axial region of the maximum diameter suffers an outer deformation, as was shown in Figure 11a,b. While increasing the inner atmospheric pressure gradually from 0 to 1400 kPa, the tip of the single-ended microbubbles suffers an expanded outward force and moves to the outer direction. On the contrary, the axial region of the maximum diameter moves to the opposite direction.

In addition, the deformation characteristic of the tip of microbubble under different wall thickness and different inner pressure was shown in Figure 12. It could be depicted that the pressure sensitivity to inner pressure is about 1667 nm/MPa for the microbubble wall thickness of 2 μm, which was in agreement with the upper experiment data. Besides, due to the limitation of simulation, the nonlinear relationship could not be calculated which was shown in upper experiment.

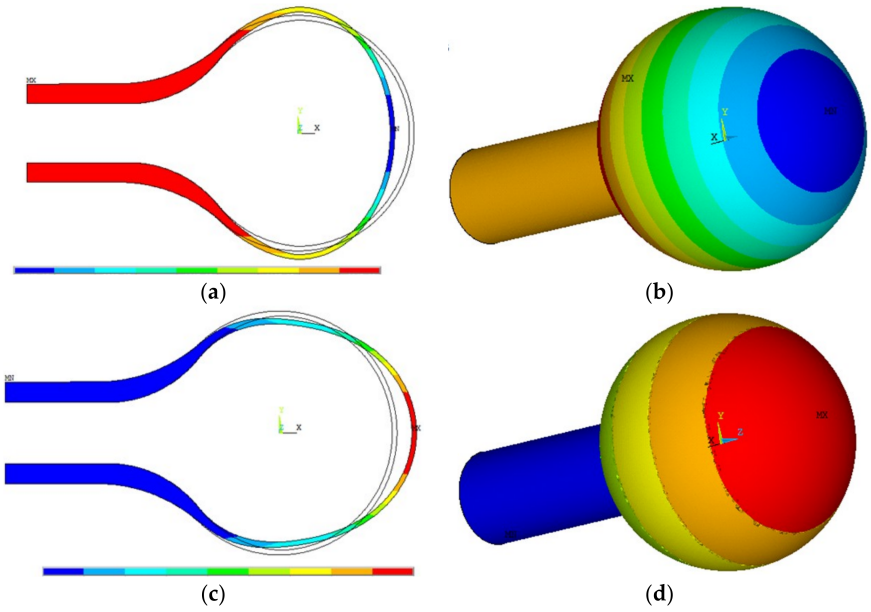

Figure 11. Deformation characteristic of the single-ended microbubble under the filling pressure of 4 and 1400 kPa. (**a**) Inner pressure: 4 kPa, 2D view; (**b**) inner pressure: 4 kPa, 3D view; (**c**) inner pressure: 1400 kPa, 2D view; (**d**) inner pressure: 1400 kPa, 3D view.

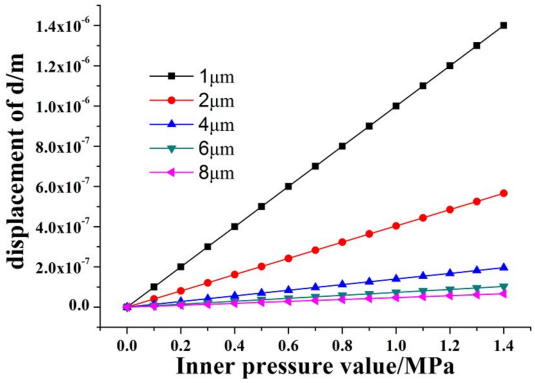

Figure 12. Relationship of bubble tip shift and iner pressure uder different wall thickness (from 1 to 8 μm).

4. Conclusions

An improved pressure-assisted discharge method is presented in this paper to fabricate the hollow core single-ended microbubble with thin wall, uniform and symmetric structure characteristics. The wall thickness can reach to the level of ~2 μm with optimized discharge parameters. For analyzing the mechanical deformation properties of fabricated single-ended microbubble, the fiber FP interference setup was used to calculate the specific deformation of microbubble under different inner pressure. The measured pressure sensitivity of sample was about 556 nm/MPa in terms of cavity length change. Besides, a high WGM quality factor up to 10^7 was also proved in this microbubble-based WGM microcavity. The ANSYS software was also used to explain the upper experimental results. This thin single-ended microbubble could be useful in building WGM microbubble devices and FP sensors.

Author Contributions: Conceptualization, G.W. (Guanjun Wang) and M.H.; Formal analysis, G.W. (Guanjun Wang); Investigation, G.W. (Gao Wang) and J.L. (Jianxun Liu); Methodology, W.G.; Supervision, G.W. (Guanjun Wang) and M.H.; Validation, J.L. (Jianxun Liu); Writing–Original Draft, G.W. (Guanjun Wang); Writing–Review & Editing, J.L. (Jinrong Liu).

Funding: This work was financially supported by Natural Science Foundation of Hainan Province (No. 617079), National Natural Science Foundation of China (Nos. 61865005 and 61762033), National Key R&D Program (No. 2016YFC0101603), National Key Technology Support Program (Nos. 2015BAH55F04 and 2015BAH55F01), Major Science and Technology Project of Hainan province (No. ZDKJ2016015), Scientific Research Staring Foundation of Hainan University (No. KYQD(ZR)1882), Shaanxi Province Science Foundation for Youths (No. 2018JQ6076).

Acknowledgments: The authors are grateful for the assistance provided by Yiping Wang (Shenzhen University).

Conflicts of Interest: The authors declare no conflict of interest.

References

1. Ward, J.M.; Dhasmana, N.; Chormaic, S.N. Hollow core, whispering gallery resonator sensors. *Eur. Phys. J. Spec. Top.* **2014**, *223*, 1917–1935. [CrossRef]
2. Liao, C.; Liu, S.; Xu, L.; Wang, C.; Wang, Y.; Li, Z.; Wang, Q.; Wang, D. Sub-micron silica diaphragm-based fiber-tip Fabry–Perot interferometer for pressure measurement. *Opt. Lett.* **2014**, *39*, 2827–2830. [CrossRef] [PubMed]
3. Liu, S.; Yang, K.; Wang, Y.; Qu, J.; Liao, C.; He, J.; Li, Z.; Yin, G.; Sun, B.; Zhou, J.; et al. High-sensitivity strain sensor based on in-fiber rectangular air bubble. *Sci. Rep.* **2015**, *5*, 7624. [CrossRef] [PubMed]
4. Berneschi, S.; Farnesi, D.; Cosi, F.; Conti, G.N.; Pelli, S.; Righini, G.C.; Soria, S. High Q silica microbubble resonators fabricated by arc discharge. *Opt. Lett.* **2011**, *36*, 3521–3523. [CrossRef] [PubMed]
5. Li, M.; Wu, X.; Liu, L.; Xu, L. Kerr parametric oscillations and frequency comb generation from dispersion compensated silica micro-bubble resonators. *Opt. Express* **2013**, *21*, 16908–16913. [CrossRef] [PubMed]
6. Li, H.; Guo, Y.; Sun, Y.; Reddy, K.; Fan, X. Analysis of single nanoparticle detection by using 3-dimensionally confined optofluidic ring resonators. *Opt. Express* **2010**, *18*, 25081. [CrossRef] [PubMed]

7. Li, M.; Wu, X.; Liu, L.; Fan, X.; Xu, L. Self-referencing optofluidic ring resonator sensor for highly sensitive biomolecular detection. *Anal. Chem.* **2013**, *85*, 9328–9332. [CrossRef] [PubMed]
8. Li, H.; Fan, X. Characterization of sensing capability of optofluidic ring resonator biosensors. *Appl. Phys. Lett.* **2010**, *97*, 011105. [CrossRef]
9. Sumetsky, M.; Dulashko, Y.; Windeler, R.S. Optical microbubble resonator. *Opt. Lett.* **2010**, *35*, 898–900. [CrossRef] [PubMed]
10. Sun, Y.; Fan, X. Optical ring resonators for biochemical and chemical sensing. *Anal. Bioanal. Chem.* **2011**, *399*, 205–211. [CrossRef] [PubMed]
11. Ward, J.M.; Yang, Y.; Nic Chormaic, S. Highly sensitive temperature measurements with liquid-core microbubble resonators. *IEEE Photonics Technol. Lett.* **2013**, *25*, 2350–2353. [CrossRef]
12. Lee, W.; Sun, Y.; Li, H.; Reddy, K.; Sumetsky, M.; Fan, X. A quasi-droplet optofluidic ring resonator laser using a micro-bubble. *Appl. Phys. Lett.* **2011**, *99*, 91102. [CrossRef]
13. Yang, Y.; Saurabh, S.; Ward, J.M.; Chormaic, S.N. High-Q, ultrathin-walled microbubble resonator for aerostatic pressure sensing. *Opt. Express* **2016**, *24*, 294–299. [CrossRef] [PubMed]
14. Watkins, A.; Ward, J.; Wu, Y.; Chormaic, S.N. Single-input spherical microbubble resonator. *Opt. Lett.* **2011**, *36*, 2113–2115. [CrossRef] [PubMed]
15. Henze, R.; Seifert, T.; Ward, J.; Benson, O. Tuning whispering gallery modes using internal aerostatic pressure. *Opt. Lett.* **2011**, *36*, 4536–4538. [CrossRef] [PubMed]
16. Yan, L.; Gui, Z.; Wang, G.; An, Y.; Gu, J.; Zhang, M.; Liu, X.; Wang, Z.; Wang, G.; Jia, P. A micro bubble structure based Fabry–Perot optical fiber strain sensor with high sensitivity and low-cost characteristics. *Sensors* **2017**, *17*, 555. [CrossRef] [PubMed]
17. Wang, G.; Huang, M.; Liu, J.; Li, Y.; Zhang, S.; Wan, X.-F.; Sardar, M.S.; Han, J.; Song, Q.; Gui, Z. Fabrication and pressure sensing characterization of an ultrathin egg-shaped microbubble. *Prog. Electromagn. Res.* **2018**, *72*, 165–174. [CrossRef]
18. Liu, S.; Sun, Z.; Zhang, L.; Fu, C.; Liu, Y.; Liao, C.; He, J.; Bai, Z.; Wang, Y.; Wang, Y. Strain-based tunable optical microresonator with an in-fiber rectangular air bubble. *Opt. Lett.* **2018**, *43*, 4077–4080. [CrossRef] [PubMed]
19. Agha, I.H.; Okawachi, Y.; Gaeta, A.L. Theoretical and experimental investigation of broadband cascaded four-wave mixing in high-Q microspheres. *Opt. Express* **2009**, *17*, 16209–16215. [CrossRef] [PubMed]
20. Liu, S. Optical fiber sensors and tunable whispering-gallery-mode resonators based on in-fiber air bubble microcavities. Ph.D. Thesis, Shenzhen University, Shenzhen, China, 2017.
21. Liu, S.; Liao, C.; Wang, Y. Optical fiber sensors based on in-fiber air bubble microcavities. *J. Appl. Sci.* **2018**, *1*, 104–147. (In Chinese)